JACS Au
AN OPEN ACCESS JOURNAL OF THE AMERICAN CHEMICAL SOCIETY

pubs.acs.org/jacsau
Article

Demagnetizing Ferromagnetic Catalysts to the Sabatier Optimal of Haber−Bosch Process

Gaomou Xu, Licheng Sun, and Tao Wang*

Cite This: JACS Au 2024, 4, 1405−1412

Read Online

ACCESS | Metrics & More | Article Recommendations | Supporting Information

ABSTRACT: Achieving the Sabatier optimal of a chemical reaction has been the central topic in heterogeneous catalysis for a century. However, this ultimate goal was greatly hindered in previous catalyst design strategies since the active sites indeed changed. Fortunately, the magneto-catalytic effect (MCE) provides a promising solution to this long-standing challenge. Recent research suggests that the performance of ferromagnetic catalysts is capable to be promoted without changing its chemical structure. Herein, we use time-dependent density functional perturbation theory (TDDFPT) calculations to elucidate that a partially demagnetized (DM) ferromagnet could be a Sabatier optimal catalyst. Using ammonia synthesis as the model reaction, we determined the activity of Cobalt at each DM state by including the magnetic thermal excitations via magnon analysis, making the 55% DM Co to the genuine Sabatier optimal. As an essential but underexcavated phenomenon in heterogeneous catalysis, the MCE will open a new avenue to design high-performance catalysts.

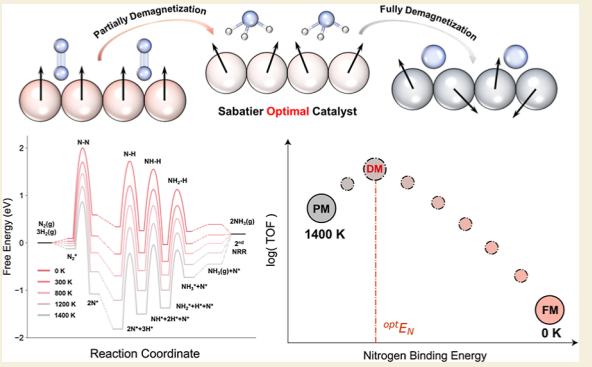

KEYWORDS: *Haber−Bosch process, Sabatier optimal, magneto-catalytic effect, TDDFPT, magnon dispersion spectrum*

INTRODUCTION

Developing high-performance catalysts is a major pursuit in today's chemical industry. In heterogeneous catalysis, the Sabatier principle demonstrates that optimal catalysts have suitable binding strengths with reaction intermediates. Moreover, a volcano-like correlation can be established between catalytic performance and E_{ads}.[1−4] Since the binding strength of adsorbates (E_{ads}) is highly related to the electronic structures (e.g., the density of states of d-electrons) of the solid catalysts,[5,6] effective design strategies as alloying,[7] strain,[8] defect engineering,[9] and confinement[10,11] are performed to tuning this essential quantity. However, it is quite challenging to separate the electronic and geometric structure of a chemical system.[4] Thus, these modifications can lead to reconstructions of the active center and ultimately establish a different reactivity trend for the newly designed structures.[3,4,12] Strictly speaking, none of the classical Sabatier volcanos have been truly approached underneath chemical and materials engineering, whereas it is more adequate to be described as a new Sabatier volcano. As a result, the regularities summarized from classical trends are insufficient to predict the performance of novel materials. This greatly limits the rational and systematic approach to the design of catalysts guided by theory.

How to alter the catalyst's electronic configuration while preserving the active site's structure is still an open question. As a crucial intrinsic property of the electron, spin is one of the ideal options. Several researchers have discussed the relationship between the on-site magnetic moment and catalytic performance.[13−17] However, in heterogeneous catalysts, not only the on-site spin state but also the interatomic magnetic order affects the system. For example, the ferromagnetic (FM) order can collapse into paramagnetic (PM) order after a second-order FM−PM phase transition (Figure 1a−d), while the chemical structure remains the same.[18,19] This results in a significant variation in reactivity around the Curie point (T_C) of the FM material, which is known as the magneto-catalytic effect (MCE).[20] Previously, we have theoretically investigated the MCE on the Haber−Bosch (H−B) process.[21] As shown in Figure 1e, the PM Co (the leftmost gray circle) is located at a higher place in the ammonia synthesis volcano than its FM counterpart (the rightmost pink circle). However, only the fully FM and fully PM states have been discussed before. Currently, we notice that the Curie transition is continuous with a series of intermediate states. Since Co indeed crosses over the reaction volcano during the Curie transition, an interesting scientific question arose: is there a partially

Received: December 10, 2023
Revised: February 21, 2024
Accepted: February 22, 2024
Published: March 12, 2024

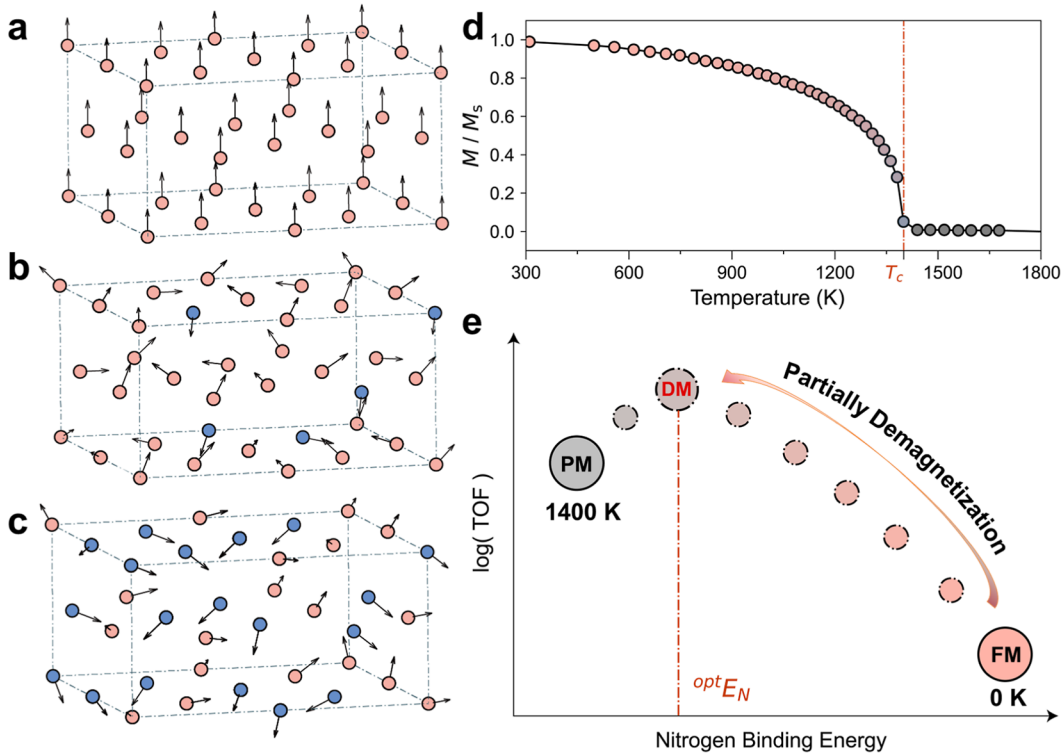

Figure 1. Curie phase transition and its influence on catalytic reactions. (a−c) Schematic diagram of the Curie phase transition process. The circles represent atomic sites in a metallic crystal, while the arrows indicate the local magnetic moments at each site. The atomic sites that are spin-up and spin-down along the *z*-direction are pink and blue, respectively. At absolute 0 K (a), the metal is fully FM, where all the magnetic moments are exactly parallel. At a finite temperature below T_C (b), the parallel alignment of the magnetic moments is disturbed by thermal fluctuation but still exhibits positive magnetization. At temperatures above T_C (c), the metal becomes totally PM where all magnetic moments orient randomly. (d) Experimentally measured temperature-dependent reduced magnetization ($m \equiv M/M_s$) for Co as fitted by Kuz'min's equation.[30] (e) Illustrative Sabatier volcano for ammonia synthesis on Co at different magnetic states. The optimal nitrogen-binding energy ($^{opt}E_N$) is shown as a red dashed line. The pink and gray circles in (d,e) represent FM and PM Co, respectively, while the colors in between pink and gray indicate partial demagnetization phases.

demagnetized (DM) status between fully FM and PM phases that could achieve the genuine Sabatier optimal (Figure 1e)?

Herein, we developed a simple and practical procedure to identify the interaction between the adatoms and the DM surface, which could not be appropriately described by standard density functional theory (DFT) calculations.[22,23] An ab initio treatment of spin fluctuations was performed with the consideration of low-lying magnetic excitations. As a compromise between computational cost and accuracy, the time-dependent density functional perturbation theory (TDDFPT) has been applied to calculate the magnon spectrum of the reacting surfaces.[24,25] With this property, the temperature dependence of the adsorbate binding energy (E_{ads}) can be quantified, and an optimal reaction temperature (^{opt}T) can be theoretically determined. At the predicted ^{opt}T, the FM catalyst could be partially DM to approach the top of the Sabatier volcano.

In this work, the H−B process has been chosen as the model reaction to illustrate the aforementioned framework due to its well-established reaction mechanism.[26−29] As a result, 55% DM Co could be the ultimate metallic catalyst for ammonia synthesis. We further anticipate that any FM materials crossing over a reaction volcano during the Curie transition have the potential to be the optimal catalyst at a reaction temperature right below its T_C. Our finding provides a simple strategy to promote FM catalysts to the Sabatier optimal, which will provide a new dimension for investigating the heterogeneous catalysis and corresponding catalyst design.

COMPUTATIONAL METHODS

Electronic Structure Calculation

All calculations were performed using the periodic plane-wave-based DFT method as implemented in Quantum Espresso package[31−33] with fully relativistic norm-conserving pseudopotentials from the PseudoDojo library.[34] Kohn−Sham spinor wave functions were expanded in plane waves (PW) up to a kinetic energy cutoff of 70 Ry, while the charge and magnetization densities and potentials were expanded in PWs with the cutoff 4 times larger than that for wave functions. The local spin density approximation (LSDA) was used for the exchange−correlation functional. The $(000\bar{1})$ facet of hcp Co was simulated using 4-layer 2 × 2 supercells with the topmost two layers relaxed and the bottom two layers constrained. The first Brillouin zone has been sampled with a uniform *k*-point mesh centered at the Γ point of size 16 × 16 × 10 for bulk and 8 × 8 × 1 for the slabs. We have used a Gaussian smearing technique with a broadening parameter of 0.01 Ry. A vacuum layer of 15 Å was set between periodically repeated slabs for the normal surfaces without confinement. Spin polarization was included for the FM state of Co, while the DM and PM energetics were derived from magnetically induced thermal excitations. The PM state has also been simulated by the nonspin polarized (NSP) calculations for comparision.

Magnon Spectrum Calculation

The magnon dispersion spectrum of clean and nitrogen-binding slabs of the hcp Co $(000\bar{1})$ facet along the Γ−M high symmetry path in the

https://doi.org/10.1021/jacsau.3c00785
JACS Au 2024, 4, 1405−1412

Brillouin zone has been calculated. Spin susceptibility $\chi(q,q;\omega)$ for the two slabs has been calculated on the following points: (1/8, 1/8, 0), (3/16, 3/16, 0), (1/4, 1/4, 0), (3/8, 3/8, 0), (1/2, 1/2, 0). The spin susceptibility matrix $\chi(q,q;\omega)$ is accessible from the linear-response theory. The corresponding calculations have been implemented by turboMagnon code.[24,25]

Microkinetic Modeling

The turnover frequency (TOF), as well as the reaction kinetics of ammonia synthesis, has been solved by microkinetic modeling (MKM) with CatMAP code.[35] The reaction rate for each elementary step can be expressed as

$$r_i = k_i^{\mathrm{f}} \prod_m \theta_{im} \prod_m p_{im} - k_i^{\mathrm{r}} \prod_n \theta_{in} \prod_n p_{in} \quad (1)$$

where r_i are the rates, $k_i^{\mathrm{f/r}}$ are the forward/reverse rate constants, $\theta_{im/in}$ are the coverage of the surface species m/n, and $p_{im/in}$ are the pressure of the gas-phase reactants and products m/n for each elementary reaction step i.

The details and derivations of the calculations can be found in the Supporting Information.

RESULTS AND DISCUSSION

Temperature-Dependent Magneto-Catalytic Effect

The MCE indicates that chemical reactions on the FM catalyst could behave differently after the Curie phase transition. This interesting phenomenon was first observed by Hedvall et al. in the N_2O decomposition reaction over Ni.[20] Unfortunately, further exploration of MCE was severely hindered by the lack of appropriate experimental techniques and theoretical methods in the 1900s. Within the picture of localized spins, the PM state can be represented as the random orientation of the magnetic moments among different atoms, which is known as the disordered local moment (DLM) model.[36−40] However, a basic assumption of the DLM model is that the time scale of local spin fluctuation is less than that of the typical time of electron hopping between atoms. As a result, the itinerant magnets (typically Fe, Co, and Ni) with delocalized d-electron bands[41,42] cannot be appropriately described by the DLM−PM treatment.[43,44]

One of the oldest and most intensive topics in magnetism was its origin in 3d transition metals.[45] While most classical models for magnetism assume localized spins, the observation of the d-electron Fermi surface in Fe and Ni indicates an itinerant nature of electronic bands. Based on mean-field treatment on electrons, the Stoner theory, as well as its ab initio version—the spin-polarized band theory, provides a reasonable description for the magnetic ground state of itinerant magnets. At the fully itinerant limit, the Stoner theory predicts a demagnetization through spin-flips until a "non-magnetic" PM state is achieved, which inspires the idea of simulating PM states with NSP calculations.[46−50] In 2004, the case of carbon segregation−dissolution on pure Ni was reinvestigated with the aid of NSP−DFT calculations,[51] and the results show a distinct variation in carbon binding energy, which accords well with experiments.[52,53]

However, neither the localized nor itinerant pictures can reflect the magnetic properties in real materials, which exist in an intermediate regime between the two pictures. Take Fe, Co, and Ni as examples, on the one hand, their noninteger Bohr magneton number accords well with the Stoner theory. On the other hand, the finite exchange splitting in spin-resolved resonant photoemission suggests the existence of local moments in their PM states.[54] The dual localized-itinerant behavior of FM 3d metals indicates that, in fact, none of the DLM-based or NSP treatments is "exact" for itinerant paramagnetism.[43] As a result, one can only compare the accuracy and efficiency of these methods rather than judge their quality and rationality. In practice, the calculations obtained from these methods should be carefully compared to experiments,[55] and whether they can be used to represent the PM states of itinerant magnets is still an open question.[23] Recently, we have revisited the MCE on the H−B process over Fe, Co, and Ni metals.[21] According to our results, the PM phases have much lower nitrogen (N_2) dissociative energy barriers (E_{N-N}) than their FM counterparts. The atomic binding energies (E_N and E_H) and molecular adsorption energies (E_{NxHy}) also decrease with different magnitudes. Meanwhile, the active sites and scaling relations are conserved along MCE since the Curie transition is a second-order phase transition. This indicates that, in principle, our ultimate goal of discovering an optimal catalyst could be achieved by refining the picture of MCE.

Approaching the Sabatier optimal needs to release us from the limited static description of MCE, where only the fully FM and PM states could be calculated. However, the Curie transition is a continuous process along a wide temperature range, e.g., 1400 K for Co. As shown in Figure 1d, the reduced magnetization (m) will gradually decrease with the increasing temperature and eventually vanishes at T_C. In our previous study, the complete phase transition process has been simplified into two individual points, i.e., the FM as the initial point and the PM as the final point. In fact, at temperatures between 0 K and T_C, the FM material is at a partially DM state with a $0 < m < 1$ (Figure 1b), but all the relative information was neglected. It is worth noting that the chemical structures of these DM states are also equivalent to those of the FM state, which indicates the scaling relations are still conserved. This inspired us to anticipate that E_{ads} of reaction intermediates on FM catalysts will decrease smoothly along with the collapsing magnetic order. As shown in Figure 1e, the temperature dependence of the MCE could be established. At finite temperatures, the FM material will be partially DM, and the intrinsic catalytic performance of the catalyst should be changed from the FM state to the PM state along the Sabatier volcano. Then, an interesting question is out: is it possible to identify a DM state with a superior performance?

This scenario becomes possible if the FM material crosses over the Sabatier volcano during the Curie transition. By modulating the reaction temperature T, a proper DM state can exhibit higher reactivity than both the FM and the PM states and even approach the Sabatier optimal. Now, we first perform a qualitative analysis for a case study (the H−B process on Co) to illustrate the above discussions. As shown in Figure 2, the nitrogen molecules are hardly adsorbed and activated on the FM Co (the topmost pink line), indicating that the FM Co is a weak-binding catalyst for ammonia synthesis. In contrast, the strong-binding PM Co would be limited by hydrogenation steps and desorption of the product (the bottommost gray line). With the simple assumption that E_N will gradually decrease from the FM state with ${}^{\mathrm{FM}}E_N$ to the PM state with ${}^{\mathrm{PM}}E_N$, an appropriate DM state with optimal nitrogen-binding energy (${}^{\mathrm{opt}}E_N$) could exhibit a significant catalytic rate and eventually achieve the top of the Sabatier volcano (Figure 1e). The ultimate Sabatier volcano has been achieved with a description of the temperature-dependent MCE.

https://doi.org/10.1021/jacsau.3c00785
JACS Au 2024, 4, 1405−1412

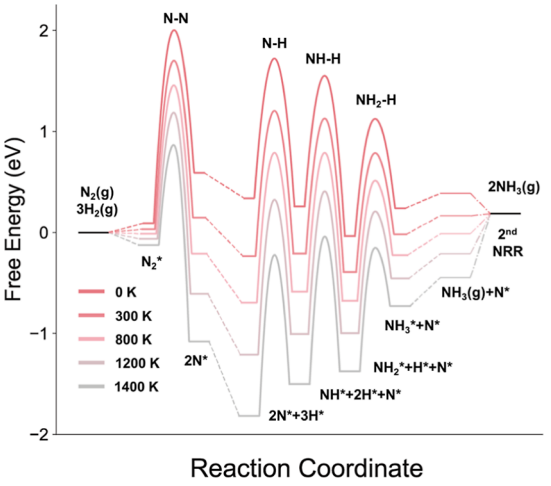

Figure 2. Calculated free energy diagram (673 K, 100 bar) for ammonia synthesis on Co at different DM states. The color of the lines indicates the temperature that could demagnetize the Co to a specific DM state. Asterisks denote adsorbed surface species, and zero energy is defined as the total free energy of the respective clean surface plus reactants in the gas phase.

Temperature Dependence of Adsorbate Binding Energy

In principle, modulating MCE is an elegant strategy to achieve the true optimal of the Sabatier volcano. However, the catalytic properties for each DM state should be properly described, which requires techniques other than standard DFT.[22,23] Since the decrease in m originates from thermal fluctuations, the issue could be addressed by directly involving the thermodynamics of ferromagnetism. Considering a magnetic contribution in thermal excitation energy, the binding energy (E_{ads}) at a given temperature of T can be represented as

$$\begin{aligned} E_{ads}(T) &= E_{M\text{-}ads}(T) - E_M(T) \\ &= [E_{M\text{-}ads}(0) + U_{M\text{-}ads}(T)] - [E_M(0) + U_M(T)] \\ &= [U_{M\text{-}ads}(T) - U_M(T)] + E_{ads}(0) \end{aligned} \tag{2}$$

where E_M and $E_{M\text{-}ads}$ are the raw DFT calculation energy of clean metal slab and adsorbate-bound metal slab. The reference energies of the atomic species are neglected here for simplicity. The U_M and $U_{M\text{-}ads}$ are the magnetically induced thermal excitation energy of the corresponding slabs, and thus $U(0) = 0$. It is noted that U is a temperature-dependent term that can be viewed as a magnetic contribution to free energy. However, to compare the relative performance of a series of

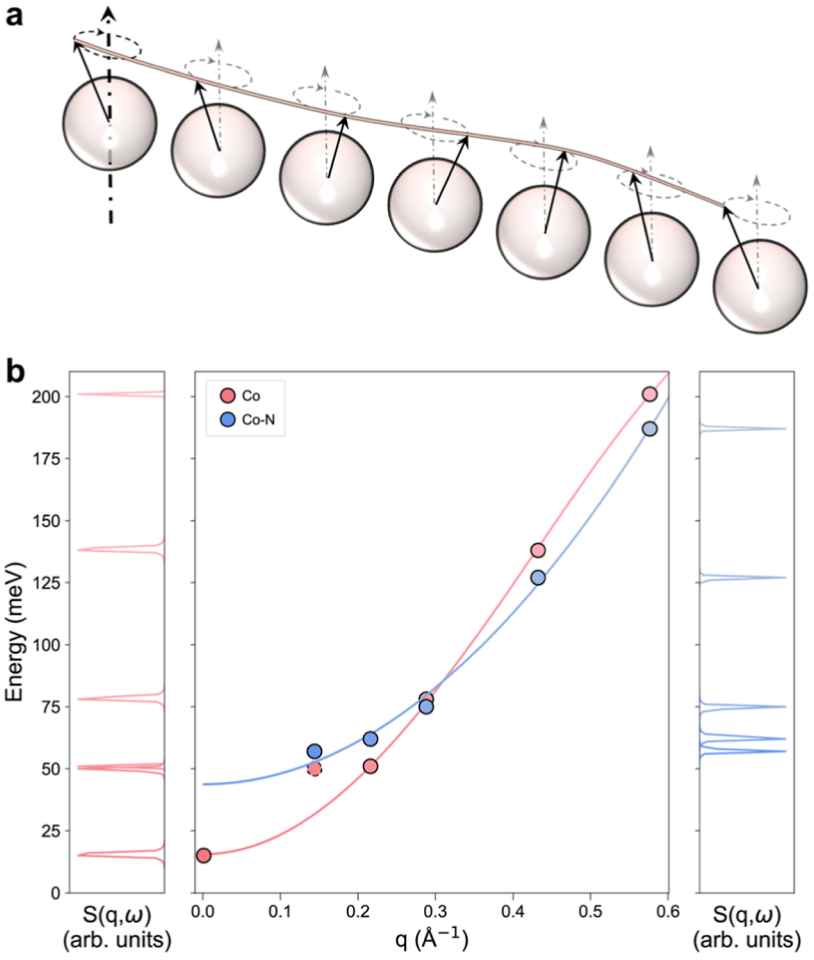

Figure 3. (a) Schematic illustration of the magnon. The gray dashed arrows and black solid arrows indicate the magnetic moment alignment in a fully FM state, and a normal mode of spin-wave, respectively. (b) Calculated magnon dispersion spectrum along the (Γ−M) path in the first Brillouin zone of clean Co (pink) and N-binding Co (blue). The side panels represent the frequency response of the magnon modes.

https://doi.org/10.1021/jacsau.3c00785
JACS Au 2024, 4, 1405−1412

DM states under the same reaction conditions, we have embedded U into E_{ads}. The nonmagnetic contribution to free energy has been considered independently. Then, the variation in binding energy ΔE_{ads} induced by the increasing temperature can be represented as

$$\Delta E_{ads}(T) = E_{ads}(T) - E_{ads}(0) = U_{M\text{-}ads}(T) - U_M(T) \quad (3)$$

Now the remaining question is to specifically express the magnetic thermal excitation energy $U_{M\text{-}ads}(T)$ and $U_M(T)$. This can be implemented by directly involving the temperature-dependent spin fluctuations.[56,57] Unlike the high-lying Stoner excitations, the introduction of magnons can describe the low-lying collective oscillations among magnetic moments as shown in Figure 3a.[49,58,59] The $U(T)$ of the system can be referred to as the total energy of excited magnons (see Supporting Information Note 4).

Here, we still focus on the H−B process due to the well-established reaction mechanism,[26−29] where the nitrogen-binding energy (E_N) is a sufficient descriptor to evaluate the reactivity of the ammonia production.[7,10] Then, the Co catalyst is chosen to illustrate the potential of MCE to reach the Sabatier optimal of the H−B volcano. We have performed structural optimization for hcp Co bulk and constructed 4-layer Co (0001) slabs with and without an atomic nitrogen binding. The magnon excitation spectrum of clean Co slab (Co) and N-bonded Co slab (Co−N) has been calculated by the Liouville−Lanczos-TDDFPT approach.[24,25] As shown in Figure 3b, the magnon spectrum of Co is lower than the Co−N at a low energy range, which indicates that the magnon properties of clean Co are disturbed by the nitrogen adatom (Figure 3a).

According to eq 3, the variation in nitrogen-binding energy, $\Delta E_N(T) = E_N(T) - E_N(0) = U_{Co-N}(T) - U_{Co}(T)$, has been calculated. Noteworthy, the calculated ΔE_N at T_C is 0.366 eV while the NSP DFT result is 0.356 eV, which indicates the NSP calculation could provide reasonable predictions for the itinerant Co. To improve the transferability of the quantity along different calculations, $\Delta E_N(T)$ and T are both reduced to their value at T_C by defining $\Delta\varepsilon_N(\tau) = \Delta E_N(T)/\Delta E_N(T_C)$ and $\tau = T/T_C$, and the corresponding results are shown in Figure 4a. As $E_N(0)$ refers to the undisturbed nitrogen-binding energy of fully FM Co ($^{FM}E_N$), we can observe $\Delta\varepsilon_N(0) = 0$ since the thermal excitation energies $U_{Co}(0) = U_{Co-N}(0) = 0$. When $T > 0$, $\Delta\varepsilon_N$ monotonically increases with T since $U_{Co}(T)$ is higher than $U_{Co-N}(T)$ (Figure S4). At the upper limit $T = T_C$, we have $\Delta\varepsilon_N(1) = 1$, and similar to $E_N(0) = {}^{FM}E_N$, $E_N(T_C)$ should be equivalent to $^{PM}E_N$, and hence $\Delta E_N(T_C)$ can be represented by $^{PM}E_N - {}^{FM}E_N$. The nitrogen-binding energy can also be expressed as

$$E_N(T) = {}^{FM}E_N + \Delta\varepsilon_N(\tau)\cdot({}^{PM}E_N - {}^{FM}E_N) \quad (4)$$

Herein, $\Delta\varepsilon_N(\tau)$ can be obtained from the model system, and $^{FM}E_N - {}^{PM}E_N$ can be taken from static DFT calculations of the extended system.

Achieving Sabatier Optimal by Demagnetizing Ferromagnetic Catalysts

Based on the established E_N−T relationship, we can now quantitatively analyze the demagnetization of catalysts in the H−B process. As shown in Figure 2, we have evaluated the free energy diagram of the FM Co and PM Co, as well as three DM Co states in between them. For a given temperature, the E_N and E_{N-N} of these DM states are extended from the FM and PM states according to eq 4, while all other binding energies and transition energies are determined by the scaling relations.[21] Noteworthy, in Figure 2, we have assumed that all magnetic states of Co with different m could exist at the same reaction temperature and compared their intrinsic reactivities at the same reaction condition. Here, the magnetic contribution on free energy has been treated under the corresponding demagnetization temperature, while the non-magnetic contribution on free energy has been treated under the reaction temperature (673 K). The free energy diagram for each state at the corresponding temperature is shown in Figure S1. Obviously, one of the DM states will maintain a perfect balance between activation of the reactant and desorption of the product, which will eventually present an optimal reaction rate.

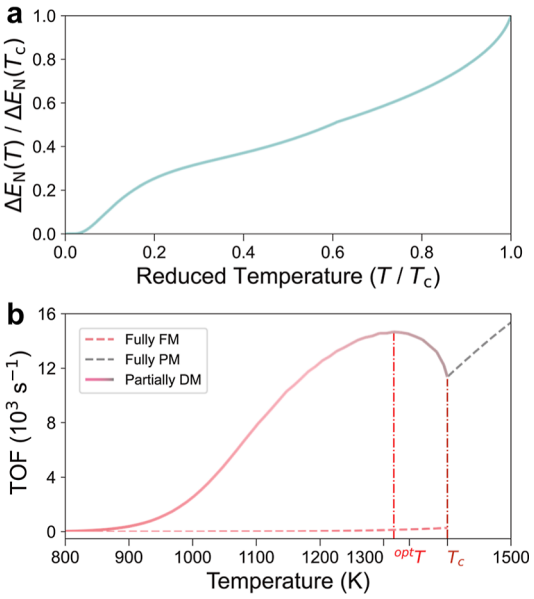

Figure 4. Influence of magnetic excitation energy on catalytic performance. (a) Calculated temperature-dependent variation in the nitrogen-binding energy $\Delta E_N(T)$. Both $\Delta E_N(T)$ and T are reduced by referring to their value at the Curie point T_C. (b) Calculated temperature-dependent TOF for ammonia synthesis on Co considering the demagnetization process. The dashed pink and gray lines represent the TOF of fully FM and PM states, respectively. The solid line indicates the TOF of partially DM Co. The optimal temperatures ^{opt}T and T_C are shown as red dashed lines.

Besides discussing the relative catalytic performance of different magnetic states of Co, we can also describe the whole process from a more realistic viewpoint. At absolute 0 K, the Co is fully FM, i.e., $m(0) = 1$, and the nitrogen bind energy is $E_N(0) = {}^{FM}E_N$. At $0 < T < T_C$, the Co could be partially DM into a DM state with $0 < m(T) < 1$, as well as $^{PM}E_N < E_N(T) < {}^{FM}E_N$. At temperatures above T_C, the Co is fully DM into the PM state with $m(T_C) = 0$, while $E_N(T_C)$ is equivalent to $^{PM}E_N$. Thus, the reactivity of Co at finite temperatures should be determined with energetics for the corresponding DM state. Furthermore, within the temperature-dependent reactivity, an optimal reaction temperature ^{opt}T which demagnetizes the Co into $m(^{opt}T) = {}^{opt}m$ can be determined.

As shown in Figure 4b, we calculated the overall temperature-dependent reactivities of Co, where a magnetic term is included in the temperature dependence of free energies (Figure S1). Since the simulation temperature range is as high

https://doi.org/10.1021/jacsau.3c00785
JACS Au 2024, 4, 1405−1412

as 1000 K, thermal excitations of phonons and vibration modes are very important. Here, we have introduced the temperature dependence of spin-wave stiffness constant D to implicitly include the phonon-magnon, as well as phonon−phonon, magnon−magnon interactions (see Supporting Information Note 4), while the vibration modes of adsorbates themselves have been taken into account in the free energy and MKM. Noteworthy, the MKM predictions on reaction kinetics, especially the value of TOF, may be quantitatively inaccurate at sufficiently high temperatures due to the thermal fluctuations on the catalytic interface, and thus the number of active sites, the reaction pathway, and the apparent activation barrier can be significantly changed.[60] However, our article focused on emphasizing the relative performance between the DM states and the PM states. Since the working condition of our targeted DM state is quite close to the T_C, we believe our main conclusion will not be affected by the consideration of all aforementioned discussions.

According to the results, the omission of the demagnetization process greatly underestimates the reactivity of Co at a high-temperature scope. We can determine an optimal temperature ${}^{opt}T$ as 1315 K, which can appropriately demagnetize the catalyst so that it can be exactly located at the top of the Sabatier volcano. At temperatures below ${}^{opt}T$, the reaction rate gradually increases to the theoretical limit $r_{opt} = r({}^{opt}T) = 14.7 \times 10^3\ s^{-1}$ and then decreases to the reactivity of the PM phase until the reaction condition reaches T_C. According to Figure 1d, the reduced magnetization of Co at ${}^{opt}T$ can be evaluated as $m = 0.45$, which indicates that $1 - m = 55\%$ DM Co could be the exclusive Sabatier optimal for ammonia synthesis. Although the predicted ${}^{opt}T$ for the H−B process on Co is dramatically high, it is worth mentioning that the mechanism we demonstrated in this work is universal for FM materials. In more ideal systems where ${}^{FM}E_N$ and ${}^{PM}E_N$ are located almost symmetrically along the ${}^{opt}E_N$, or the T_C itself is near room temperature, the ${}^{opt}T$ could be relatively lower. In general, any FM material that crosses over the Sabatier volcano during the Curie phase transition has the potential to be the optimal catalyst at a reaction temperature that is right below its T_C.

CONCLUSIONS

In this work, we first theoretically refine the physical picture and the working mechanism of the MCE. Then, we discuss a specific case with the FM state at the weak-binding and PM state at the strong-binding legs of the Sabatier volcano, which opens an exciting avenue to achieve a genuine Sabatier optimal by partially demagnetizing the FM catalysts. Here, we developed a simple procedure to determine the temperature dependence of the adsorbate binding energies of the FM catalysts. The issue is addressed by directly involving the magnetically induced thermal excitation energy via the magnon spectrum calculated from TDDFPT. Using ammonia synthesis as the model reaction, we demonstrate the activity of the Co catalyst at each DM state, where 55% DM Co is identified as the Sabatier optimal. We believe our demonstrations not only thoroughly conclude the physical basics, fundamental working mechanism, and theoretical potential of MCE, but also dramatically extend its practical applications in heterogeneous catalysis. We anticipate that our case study will provide a new possibility for rational catalyst design.

ASSOCIATED CONTENT

Data Availability Statement

Computational Methods, the data that support the plots within this paper, and other findings of this study are available in Supporting Information. The code used to perform the microkinetics modeling of this work is available at https://github.com/SUNCAT-Center/catmap.

Supporting Information

The Supporting Information is available free of charge at https://pubs.acs.org/doi/10.1021/jacsau.3c00785.

Computational methods, Supporting Information Notes 1−5, and Supporting Information Figures S1−S5 are available in the text (PDF)

AUTHOR INFORMATION

Corresponding Author

Tao Wang − *Center of Artificial Photosynthesis for Solar Fuels and Department of Chemistry, School of Science and Research Center for Industries of the Future, Westlake University, Hangzhou 310030 Zhejiang Province, China; Institute of Natural Sciences, Westlake Institute for Advanced Study, Hangzhou 310024 Zhejiang Province, China; Division of Solar Energy Conversion and Catalysis at Westlake University, Zhejiang Baima Lake Laboratory, Hangzhou 310000 Zhejiang Province, China;* orcid.org/0000-0003-4451-2721; Email: twang@westlake.edu.cn

Authors

Gaomou Xu − *Center of Artificial Photosynthesis for Solar Fuels and Department of Chemistry, School of Science and Research Center for Industries of the Future, Westlake University, Hangzhou 310030 Zhejiang Province, China; Institute of Natural Sciences, Westlake Institute for Advanced Study, Hangzhou 310024 Zhejiang Province, China*

Licheng Sun − *Center of Artificial Photosynthesis for Solar Fuels and Department of Chemistry, School of Science and Research Center for Industries of the Future, Westlake University, Hangzhou 310030 Zhejiang Province, China; Institute of Natural Sciences, Westlake Institute for Advanced Study, Hangzhou 310024 Zhejiang Province, China; Division of Solar Energy Conversion and Catalysis at Westlake University, Zhejiang Baima Lake Laboratory, Hangzhou 310000 Zhejiang Province, China;* orcid.org/0000-0002-4521-2870

Complete contact information is available at: https://pubs.acs.org/10.1021/jacsau.3c00785

Author Contributions

T.W. led and supervised this project; G.X. performed all calculations used in this work and data analysis; all authors discussed the results and commented on the manuscript.

Notes

The authors declare no competing financial interest.

ACKNOWLEDGMENTS

This work was supported by the National Natural Science Foundation of China (22273076 to T.W.) and the National Key Research and Development Program of China (2022YFA0911900 to L.S.); T.W. and L.S. thanks for the start-up packages from Westlake University and the Kunpeng

research fund (to L.S.) from Zhejiang Province. We thank the Research Center for Industries of the Future (RCIF) at Westlake University for supporting this work. We thank Westlake University HPC Center for computation support.

REFERENCES

(1) Norskov, J. K.; Bligaard, T.; Rossmeisl, J.; Christensen, C. H. Towards the computational design of solid catalysts. *Nat. Chem.* **2009**, *1* (1), 37−46.
(2) Medford, A. J.; Vojvodic, A.; Hummelshøj, J. S.; Voss, J.; Abild-Pedersen, F.; Studt, F.; Bligaard, T.; Nilsson, A.; Nørskov, J. K. From the Sabatier principle to a predictive theory of transition-metal heterogeneous catalysis. *J. Catal.* **2015**, *328*, 36−42.
(3) Xu, G.; Cai, C.; Zhao, W.; Liu, Y.; Wang, T. Rational design of catalysts with earth-abundant elements. *Wiley Interdiscip. Rev.: Comput. Mol. Sci.* **2022**, *13* (4), No. e1654.
(4) Pérez-Ramírez, J.; López, N. Strategies to break linear scaling relationships. *Nat. Catal.* **2019**, *2* (11), 971−976.
(5) Hu, P.; King, D. A.; Lee, M. H.; Payne, M. C. Orbital mixing in CO chemisorption on transition metal surfaces. *Chem. Phys. Lett.* **1995**, *246* (1−2), 73−78.
(6) Hammer, B.; Nørskov, J. K. Theoretical surface science and catalysis—calculations and concepts. *Advances in Catalysis*; Academic Press, 2000; Vol. *45*, pp 71−129.
(7) Jacobsen, C. J. H.; Dahl, S.; Clausen, B. S.; Bahn, S.; Logadottir, A.; Nørskov, J. K. Catalyst Design by Interpolation in the Periodic Table: Bimetallic Ammonia Synthesis Catalysts. *J. Am. Chem. Soc.* **2001**, *123* (34), 8404−8405.
(8) Khorshidi, A.; Violet, J.; Hashemi, J.; Peterson, A. A. How strain can break the scaling relations of catalysis. *Nat. Catal.* **2018**, *1* (4), 263−268.
(9) Ye, T.-N.; Park, S.-W.; Lu, Y.; Li, J.; Sasase, M.; Kitano, M.; Tada, T.; Hosono, H. Vacancy-enabled N2 activation for ammonia synthesis on an Ni-loaded catalyst. *Nature* **2020**, *583* (7816), 391−395.
(10) Wang, T.; Abild-Pedersen, F. Achieving industrial ammonia synthesis rates at near-ambient conditions through modified scaling relations on a confined dual site. *Proc. Natl. Acad. Sci. U.S.A.* **2021**, *118* (30), No. e2106527118.
(11) Zhao, W.; Xu, G.; He, Z.; Cai, C.; Abild-Pedersen, F.; Wang, T. Toward Carbon Monoxide Methanation at Mild Conditions on Dual-Site Catalysts. *J. Am. Chem. Soc.* **2023**, *145* (15), 8726−8733.
(12) Zhao, Z.-J.; Liu, S.; Zha, S.; Cheng, D.; Studt, F.; Henkelman, G.; Gong, J. Theory-guided design of catalytic materials using scaling relationships and reactivity descriptors. *Nat. Rev. Mater.* **2019**, *4* (12), 792−804.
(13) Munarriz, J.; Polo, V.; Gracia, J. On the Role of Ferromagnetic Interactions in Highly Active Mo-Based Catalysts for Ammonia Synthesis. *ChemPhysChem* **2018**, *19* (21), 2843−2847.
(14) Zhong, W.; Qiu, Y.; Shen, H.; Wang, X.; Yuan, J.; Jia, C.; Bi, S.; Jiang, J. Electronic Spin Moment As a Catalytic Descriptor for Fe Single-Atom Catalysts Supported on C2N. *J. Am. Chem. Soc.* **2021**, *143* (11), 4405−4413.
(15) He, M.; Chen, X.; Zhou, Y.; Xu, C.; Li, X.; Luo, Q.; Yang, J. A First-Principles Study of Regulating Spin States of MoSi2N4 Supported Single-Atom Catalysts Via Doping Strategy for Enhancing Electrochemical Nitrogen Fixation Activity. *J. Phys. Chem. Lett.* **2023**, *14*, 7100−7107.
(16) He, Z.-D.; Tesch, R.; Eslamibidgoli, M. J.; Eikerling, M. H.; Kowalski, P. M. Low-spin state of Fe in Fe-doped NiOOH electrocatalysts. *Nat. Commun.* **2023**, *14* (1), 3498.
(17) Do, V.-H.; Lee, J.-M. Orbital Occupancy and Spin Polarization: From Mechanistic Study to Rational Design of Transition Metal-Based Electrocatalysts toward Energy Applications. *ACS Nano* **2022**, *16* (11), 17847−17890.
(18) Curie, P. Sur la symétrie dans les phénomènes physiques, symétrie d'un champ électrique et d'un champ magnétique. *J. Phys. Theor. Appl.* **1894**, *3* (1), 393−415.
(19) Landau, L. The Theory of Phase Transitions. *Nature* **1936**, *138* (3498), 840−841.
(20) Hedvall, J.; Hedin, R.; Persson, O. Ferromagnetic transformation and catalytic activity. *Z. Phys. Chem. Abt. B* **1934**, *27*, 196.
(21) Xu, G.; Cai, C.; Wang, T. Toward Sabatier Optimal for Ammonia Synthesis with Paramagnetic Phase of Ferromagnetic Transition Metal Catalysts. *J. Am. Chem. Soc.* **2022**, *144* (50), 23089−23095.
(22) Abrikosov, I. A.; Ponomareva, A. V.; Steneteg, P.; Barannikova, S. A.; Alling, B. Recent progress in simulations of the paramagnetic state of magnetic materials. *Curr. Opin. Solid State Mater. Sci.* **2016**, *20* (2), 85−106.
(23) Li, K.; Fu, C.-C.; Schneider, A. Effects of magnetic excitations and transitions on vacancy formation: Cases of fcc Fe and Ni compared to bcc Fe. *Phys. Rev. B* **2021**, *104* (10), 104406.
(24) Gorni, T.; Timrov, I.; Baroni, S. Spin dynamics from time-dependent density functional perturbation theory. *Eur. Phys. J. B* **2018**, *91* (10), 249.
(25) Gorni, T.; Baseggio, O.; Delugas, P.; Baroni, S.; Timrov, I. turboMagnon—A code for the simulation of spin-wave spectra using the Liouville-Lanczos approach to time-dependent density-functional perturbation theory. *Comput. Phys. Commun.* **2022**, *280*, 108500.
(26) Ertl, G. Surface Science and Catalysis—Studies on the Mechanism of Ammonia Synthesis: The P. H. Emmett Award Address. *Catal. Rev.* **1980**, *21* (2), 201−223.
(27) Ertl, G. Elementary Steps in Heterogeneous Catalysis. *Angew. Chem., Int. Ed.* **1990**, *29* (11), 1219−1227.
(28) Jennings, J. R. *Catalytic Ammonia Synthesis: Fundamentals and Practice*; Springer Science & Business Media, 1991.
(29) Honkala, K.; Hellman, A.; Remediakis, I. N.; Logadottir, A.; Carlsson, A.; Dahl, S.; Christensen, C. H.; Nørskov, J. K. Ammonia Synthesis from First-Principles Calculations. *Science* **2005**, *307* (5709), 555−558.
(30) Kuz'min, M. D. Shape of Temperature Dependence of Spontaneous Magnetization of Ferromagnets: Quantitative Analysis. *Phys. Rev. Lett.* **2005**, *94* (10), 107204.
(31) Giannozzi, P.; Baroni, S.; Bonini, N.; Calandra, M.; Car, R.; Cavazzoni, C.; Ceresoli, D.; Chiarotti, G. L.; Cococcioni, M.; Dabo, I.; et al. QUANTUM ESPRESSO: a modular and open-source software project for quantum simulations of materials. *J. Phys.: Condens. Matter* **2009**, *21* (39), 395502.
(32) Giannozzi, P.; Andreussi, O.; Brumme, T.; Bunau, O.; Buongiorno Nardelli, M.; Calandra, M.; Car, R.; Cavazzoni, C.; Ceresoli, D.; Cococcioni, M.; et al. Advanced capabilities for materials modelling with Quantum ESPRESSO. *J. Phys.: Condens. Matter* **2017**, *29* (46), 465901.
(33) Giannozzi, P.; Baseggio, O.; Bonfà, P.; Brunato, D.; Car, R.; Carnimeo, I.; Cavazzoni, C.; De Gironcoli, S.; Delugas, P.; Ferrari Ruffino, F.; et al. Quantum ESPRESSO toward the exascale. *J. Chem. Phys.* **2020**, *152* (15), 154105.
(34) Van Setten, M. J.; Giantomassi, M.; Bousquet, E.; Verstraete, M. J.; Hamann, D. R.; Gonze, X.; Rignanese, G. M. The PseudoDojo: Training and grading a 85 element optimized norm-conserving pseudopotential table. *Comput. Phys. Commun.* **2018**, *226*, 39−54.
(35) Medford, A. J.; Shi, C.; Hoffmann, M. J.; Lausche, A. C.; Fitzgibbon, S. R.; Bligaard, T.; Nørskov, J. K. CatMAP: A Software Package for Descriptor-Based Microkinetic Mapping of Catalytic Trends. *Catal. Lett.* **2015**, *145* (3), 794−807.
(36) Hubbard, J. The magnetism of iron. *Phys. Rev. B* **1979**, *19* (5), 2626−2636.
(37) Hubbard, J. Magnetism of iron. II. *Phys. Rev. B* **1979**, *20* (11), 4584−4595.
(38) Hasegawa, H. Single-Siet Spin Fluctuation Theory of Itinerant-Electron Systems with Narrow Bands. *J. Phys. Soc. Jpn.* **1980**, *49* (1), 178−188.
(39) Hasegawa, H. Single-Site Spin Fluctuation Theory of Itinerant-Electron Systems with Narrow Bands. II. Iron and Nickel. *J. Phys. Soc. Jpn.* **1980**, *49* (3), 963−971.

https://doi.org/10.1021/jacsau.3c00785
JACS Au 2024, 4, 1405−1412

(40) Gyorffy, B. L.; Pindor, A. J.; Staunton, J.; Stocks, G. M.; Winter, H. A first-principles theory of ferromagnetic phase transitions in metals. *J. Phys. F: Met. Phys.* **1985**, *15* (6), 1337−1386.
(41) Ruban, A. V.; Shallcross, S.; Simak, S. I.; Skriver, H. L. Atomic and magnetic configurational energetics by the generalized perturbation method. *Phys. Rev. B* **2004**, *70* (12), 125115.
(42) Mugiraneza, S.; Hallas, A. M. Tutorial: a beginner's guide to interpreting magnetic susceptibility data with the Curie-Weiss law. *Commun. Phys.* **2022**, *5* (1), 95.
(43) Ruban, A. V.; Razumovskiy, V. I. Spin-wave method for the total energy of paramagnetic state. *Phys. Rev. B* **2012**, *85* (17), 174407.
(44) Chen, X.-Y.; Long, M.-Q.; Wang, Y.-P. Paramagnetic phases of two-dimensional magnetic materials. *Phys. Rev. B* **2020**, *102* (21), 214417.
(45) Moriya, T.; Takahashi, Y. Itinerant Electron Magnetism. *Annu. Rev. Mater. Sci.* **1984**, *14* (1), 1−25.
(46) Dobin, A. Y.; Duan, W.; Wentzcovitch, R. M. Magneto-structural effects and phase transition inCr2O3under pressure. *Phys. Rev. B* **2000**, *62* (18), 11997−12000.
(47) Schneider, J. M.; Sun, Z.; Mertens, R.; Uestel, F.; Ahuja, R. Ab initio calculations and experimental determination of the structure of Cr2AlC. *Solid State Commun.* **2004**, *130* (7), 445−449.
(48) Rivadulla, F.; Bañobre-López, M.; Quintela, C. X.; Piñeiro, A.; Pardo, V.; Baldomir, D.; López-Quintela, M. A.; Rivas, J.; Ramos, C. A.; Salva, H.; et al. Reduction of the bulk modulus at high pressure in CrN. *Nat. Mater.* **2009**, *8* (12), 947−951.
(49) Coey, J. M. *Magnetism and Magnetic Materials*; Cambridge University Press, 2010.
(50) Khandy, S. A.; Gupta, D. C. Structural, elastic and thermo-electronic properties of paramagnetic perovskite $PbTaO_3$. *RSC Adv.* **2016**, *6* (53), 48009−48015.
(51) Siegel, D. J.; Van Schilfgaarde, M.; Hamilton, J. C. Understanding the Magnetocatalytic Effect: Magnetism as a Driving Force for Surface Segregation. *Phys. Rev. Lett.* **2004**, *92* (8), 086101.
(52) Hamilton, J. C.; Jach, T. Structural Phase Transitions in Nickel at the Curie Temperature. *Phys. Rev. Lett.* **1981**, *46* (11), 745−748.
(53) Jach, T.; Hamilton, J. C. Reversible step rearrangement and segregation on nickel surfaces at the Curie temperature. *Phys. Rev. B* **1982**, *26* (7), 3766−3773.
(54) Kakizaki, A.; Fujii, J.; Shimada, K.; Kamata, A.; Ono, K.; Park, K. H.; Kinoshita, T.; Ishii, T.; Fukutani, H. Fluctuating local magnetic moments in ferromagnetic Ni observed by the spin-resolved resonant photoemission. *Phys. Rev. Lett.* **1994**, *72* (17), 2781−2784.
(55) Alling, B.; Marten, T.; Abrikosov, I. A. Questionable collapse of the bulk modulus in CrN. *Nat. Mater.* **2010**, *9* (4), 283−284.
(56) Staunton, J. B.; Gyorffy, B. L. Onsager cavity fields in itinerant-electron paramagnets. *Phys. Rev. Lett.* **1992**, *69* (2), 371−374.
(57) Uhl, M.; Kübler, J. Exchange-Coupled Spin-Fluctuation Theory: Application to Fe, Co, and Ni. *Phys. Rev. Lett.* **1996**, *77* (2), 334−337.
(58) Cullity, B. D.; Graham, C. D. *Introduction to Magnetic Materials*; John Wiley & Sons, 2011.
(59) Fazekas, P. *Lecture Notes on Electron Correlation and Magnetism*; World Scientific, 2008.
(60) Bonati, L.; Polino, D.; Pizzolitto, C.; Biasi, P.; Eckert, R.; Reitmeier, S.; Schlögl, R.; Parrinello, M. The Role of Dynamics in Heterogeneous Catalysis: Surface Diffusivity and N_2 Decomposition on Fe(111). *Proc. Natl. Acad. Sci. U.S.A.* **2023**, *120* (50), No. e2313023120.

https://doi.org/10.1021/jacsau.3c00785
JACS Au 2024, 4, 1405−1412